CrossMark

ORIGINAL PAPER

Solid polymer electrolytes based on Li$^+$/ionic liquid for lithium secondary batteries

Varun Kumar Singh[1] · Shalu[1] · L. Balo[1] · H. Gupta[1] · S. K. Singh[1] ·
Rajendra Kumar Singh[1]

Abstract Ionic liquid (IL)-based solid polymer electrolytes (SPEs) were synthesized by solution cast technique using polymer polyethylene oxide (PEO), lithium bis(trifluoromethane sulfonyl) imide (LiTFSI) salt, and IL 1-butyl-3-methylimidazolium bis(trifluoromethane sulfonyl) imide (BMIMTFSI). The obtained polymer electrolytes (PEO + 20 wt.% LiTFSI) + x wt.% BMIMTFSI where x = 0, 5, 10, 15, and 20 were characterized by DSC, TGA, SEM, XRD, FTIR, electrochemical impedance spectroscopy (EIS), cyclic voltammetry, chronoamperometry, and chronocharge-discharge. Ionic conductivity of optimized composition SPE (PEO + 20 wt.% LiTFSI) + 20 wt.% BMIMTFSI is ~1.5×10^{-4} S cm^{-1} at 30 °C and follows Arrhenius-type thermally activated behavior. The prepared SPEs are free-standing and flexible with excellent thermal and mechanical stabilities. SEM, XRD, and DSC studies show that the amorphicity of SPEs increases on increasing IL content due to the plasticization effect of IL. The assembled cell exhibits good electrochemical stability and cationic transference number t_{Li^+} ~0.27. The capacity of cell, Li | PEO + 20 wt.% LiTFSI + 20 wt.% BMIMTFSI | LiMn$_2$O$_4$, shows a stable cyclic performance and high Coulombic efficiency.

Introduction

Development of IL-based, Li-ion conducting polymer electrolytes is one of the advanced technologies for the fabrication of various high potential electrochemical devices such as hybrid vehicles, rechargeable batteries and supercapacitors [1–3]. Over the past decades, storage of energy has become an increasing global concern due to increasing the demand of energy worldwide and drastic increase in the cost of refined fossil fuels and the environmental issues for their use [4]. Lithium-ion batteries are widely used in various types of portable electronic devices and choice of IL-based Li-ion conducting polymer electrolyte almost fulfills most of the requirements for the rechargeable batteries. The choice of lithium metal as anode for lithium batteries is due to its high theoretical-gravimetric capacity of 3861 mAh/g, which is much higher (about 10 times) than the commercially used graphite anode (372 mAh/g) and the lowest redox potential (−3.04 V vs. standard hydrogen electrode) [5, 6]. Organic liquid electrolytes commonly employed as an electrolyte for lithium-ion batteries cause high reactivity towards Li metal and form undesirable dendrites at anodes which results in poor performance of batteries. The use of liquid electrolytes in Li-ion battery causes serious safety issues due to possible leakage of corrosive liquid, spontaneous combustion and explosion. Therefore, the Li-ion conducting solid polymer electrolytes (SPEs) can be a better alternative for abovementioned problems [7, 8]. As compared to other solid electrolyte, the polymer electrolyte membranes are better option to develop a

✉ Rajendra Kumar Singh
  rajendrasingh.bhu@gmail.com; rksingh_17@rediffmail.com

[1] Ionic Liquid and Solid State Ionics Laboratory, Department of Physics, Banaras Hindu University, Varanasi 221005, India

variety of electrochemical devices like rechargeable batteries, supercapacitors, fuel cells and actuators. Lithium-ion conducting solid polymer electrolyte based on polymer polyethylene oxide (PEO) is one of the most promising and widely studied host solid polymer matrix due to its favorable properties such as better shape and flexibility, good ionic conductivity, good film forming ability, high solvating property and reduced reactivity towards electrodes [9]. In the present study, IL-assisted, PEO-based Li-ion conducting SPE for Li-ion rechargeable batteries have been used [10, 11]. Earlier studied SPEs formed by complexing PEO with various alkali metal salts have low room temperature ionic conductivities ($\sim 10^{-6}$–10^{-8} S cm^{-1}), which limits their application in fabrication of various electrochemical devices [11]. The lower value of ionic conductivity occurs due to multiphase nature of polymer electrolytes consisting of high crystalline phase and less amorphous phase, which hinders the motion of the ions in the polymeric network. Therefore, to attain high value of ionic conductivity at room temperature, different approaches were proposed such as (a) addition of low molecular weight plasticizers/organic carbonates (e.g., ethylene carbonate (EC), propylene carbonate (PC), diethyl carbonate (DEC)), (b) composite formation by dispersing inorganic filler particles (like ZrO_2, $BaTiO_3$, Sb_2O_3, SiO_2, Al_2O_3, CNT, and TiO_2), and incorporating IL into Li-ion conducting polymeric systems [12–15]. Among these approaches, the addition of IL in polymer and polymer electrolytes is a versatile approach because IL offers many distinct advantages such as high ionic conductivity, non-flammability, low vapor pressure, good thermal stability, and broad electrochemical window [16–21]. The application of ILs in electrochemical devices, such as Li-ion batteries, not only fulfills the requirement of plasticizing salts but also offers improved thermal and electrochemical stabilities. Various ILs having cations based on imidazolium [22, 23], piperidinium [24, 25], quaternary ammonium [26], morpholinium [27] and pyrrolidinium have been explored as plasticizers for application in battery/capacitor [28, 29]. Shin et al. presented the suitability of pyrrolidinium cation-based IL N-methyl-N-propylpyrrolidinium bis(trifluoromethanesulfonylimide) (PYR$_{13}$TFSI) in Li-rechargeable battery [27–29]. However, 1-butyl-3-methylimidazolium (BMIM$^+$) cation-based ILs are less explored as electrolytes [22, 27], due to the following reported interesting properties: IL 1-butyl-3-methylimidazoliumbis(trifluoromethylsulfonyl) imide (BMIMTFSI) has cathodic limit (−2 vs. −1.5 V) and anodic limit (2.6 vs. 2.2 V), high electrochemical stability window (4.6 vs. 3.7 V), viscosity (52 cP at 20 °C vs. 63 cP at 25 °C) and high room temperature ionic conductivity (3.9 mS/cm at 20 °C vs. 1.4 mS/cm at 25 °C) [22, 27]. These parameters are improved compared to pyrrolidinium-based IL.

In the present investigation, we report the synthesis and characterization of polymer electrolyte membrane based on IL, BMIMTFSI, lithium salt/lithium bis(trifluoromethane sulfonyl) imide (LiTFSI), and polymer PEO. The effect of IL on the physicochemical properties of PEO-LiTFSI salt system have been studied in terms of their ionic conductivity, structural changes/surface morphology, complexation, phase transition temperatures, thermal stability, transference number, electrochemical potential window and charge discharge characteristics.

Experiment

The Li-ion conducting SPE membranes (PEO + 20 wt.% of LiTFSI) + x wt.% BMIMTFSI (for x = 0, 5, 10, 15, and 20) were prepared by solution cast technique as described by us earlier [30, 31]. The starting materials used for the preparation of polymer electrolytes are poly(ethyleneoxide), PEO (m.w. = 6×10^5 g/mol), lithium bis(trifluoromethanesulfonyl) imide (LiTFSI) (purity ≥99.9%), and IL BMIMTFSI of purity ≥98% procured from Sigma-Aldrich. Prior to use, lithium salt LiTFSI and IL BMIMTFSI were vacuum dried at 120 °C for 24 h and stored inside the argon-filled glove box. The thickness of all prepared solid polymeric membranes lies in the range of ~150–300 μm.

Preparation of cathode

The electrode slurry was prepared using $LiMn_2O_4$ as an active material (80 wt.%), carbon black as conductive additive (10 wt.%) and binder polyvinylidene fluoride (PVDF) (10 wt.%) in 1-methyl-2-pyrrolidinone (NMP as solvent; Sigma-Aldrich). After intimate mixing and stirring for 24 h in an Ar atmosphere, the resulting slurry was casted on aluminum foil with the help of doctor's blade and left for drying at room temperature. As a result, cathode film was put into the vacuum oven at the 110 °C for 8 h to remove any traces of NMP solvent and was pressed by applying the pressure of 1 ton with the help of hydraulic machine. Disk-shaped films were cut having diameter of 2 cm. Finally, the cell Li | (PEO + 20 wt.% LITFSI) + 20 wt.% BMIMTFSI | $LiMn_2O_4$ was assembled. The whole-cell assembly was done in a glove box filled with Ar gas (H_2O and O_2 contents less than 0.5 ppm).

Measurements

The ionic conductivity measurements of the prepared polymer electrolyte membranes were performed by electrochemical impedance spectroscopy technique using an alpha analyzer (Novocontrol) in the frequency range of 1 Hz–40 MHz. The bulk resistance (R_b) was determined from Nyquist plots. The ionic conductivity (σ) was calculated by using the following relation:

$$\sigma = \frac{\ell}{R_b A} \qquad (1)$$

where ℓ is the thickness of the sample, A is the cross-sectional area of the disk-shaped sample and R_b is the bulk resistance obtained from Nyquist plots. For temperature-dependent conductivity studies, thin disk-shaped polymeric membranes were sandwiched between two stainless steel electrodes, and the whole assembly was kept in a temperature-controlled oven and the temperature-dependent conductivity was measured by using Novotherm Alpha analyzer. The XRD profiles of the polymer electrolyte membranes were obtained using an X'Pert PRO X-ray diffractometer (PANalytical) with Cu-Kα radiation ($\lambda = 1.54$ Å) in the range of $2\theta = 10°$ to $50°$. The surface morphology of the polymeric membranes was examined with the help of scanning electron microscope model Quanta C-200.

Differential scanning calorimetry was carried out using Mettler DSC1 in the temperature range of −100 to 100 °C at a heating rate of 10 °C/min under nitrogen atmosphere. Thermogravimetric analysis (TGA) was performed on Mettler TGA/DSC1 in the temperature range of 30 to 600 °C in nitrogen atmosphere at a heating rate of 10 °C/min. FTIR spectra of the polymeric membranes were recorded with the help of Perkin-Elmer FTIR spectrometer (model RX1) from 3500 to 400 cm^{-1}.

To estimate the "electrochemical stability window" of the polymer electrolyte, we have conducted cyclic voltammetric (CV) studies using electrochemical analyzer with an AUTOLAB PGSTAT 302 N controlled by NOVA 1.10.4 software version (Metraohm Lab). The cationic and total ionic transference numbers of SPEs were determined by combining AC impedance spectroscopy and chronoamperometry ($\Delta t < 1$ ms) technique. The linear sweep voltammetry (LSV) and CV of the assembled cell Li | SPE | LiMn$_2$O$_4$ were measured at ambient temperature (~30 °C) with a scan rate of 0.01 V/s between ~0–4.5 and ~2.8–4.4 V, respectively. Two-electrode cell was assembled by sandwiching SPE between the LiMn$_2$O$_4$ cathode along with cathode current collector, Al-foil and lithium-metal anode, and then, electrochemical performance test was carried out by using chronocharge-discharge at 0.2 C rate between ~4.5 and 2.8 V.

Results and discussion

The polymer PEO is a polar and semicrystalline in nature. The polar group present in PEO, i.e., C–O–C bond, is known to form complex with many alkali metal salts and introduces ionic conductivity in it. Apart from conductivity, another important parameter which controls the ionic transport in polymer electrolytes is the degree of crystallinity. The addition of IL into PEO-LiTFSI complex system significantly changes the degree of crystallinity as observed by XRD and DSC studies.

Thermal studies

Figure 1a shows the DSC thermograms of pristine PEO and (PEO + 20 wt.% LiTFSI salt) + x wt.% of BMIMTFSI (for $x = 0, 5, 10, 15$ and 20). The pure PEO exhibits a melting peak (T_m) at 70 °C and (inset of Fig. 1a shows its magnified image) glass transition temperature at −65 °C as shown in Fig. 1 (a). When 20 wt.% LiTFSI salt was added in pristine PEO, T_m and T_g of polymer electrolyte shifted to 67 and −40 °C, respectively (see Fig. 1a (b)). It is also observed that the addition of BMIMTFSI into the PEO + 20 wt.% LiTFSI results in a further decrease in both T_g and T_m (as shown in Fig. 1a (c–f)) due to the plasticization effect of the IL and increased dissociation of ion pairs in the polymeric membranes [32, 33]. The degree of crystallinity (X_c) of these SPEs has also been found to
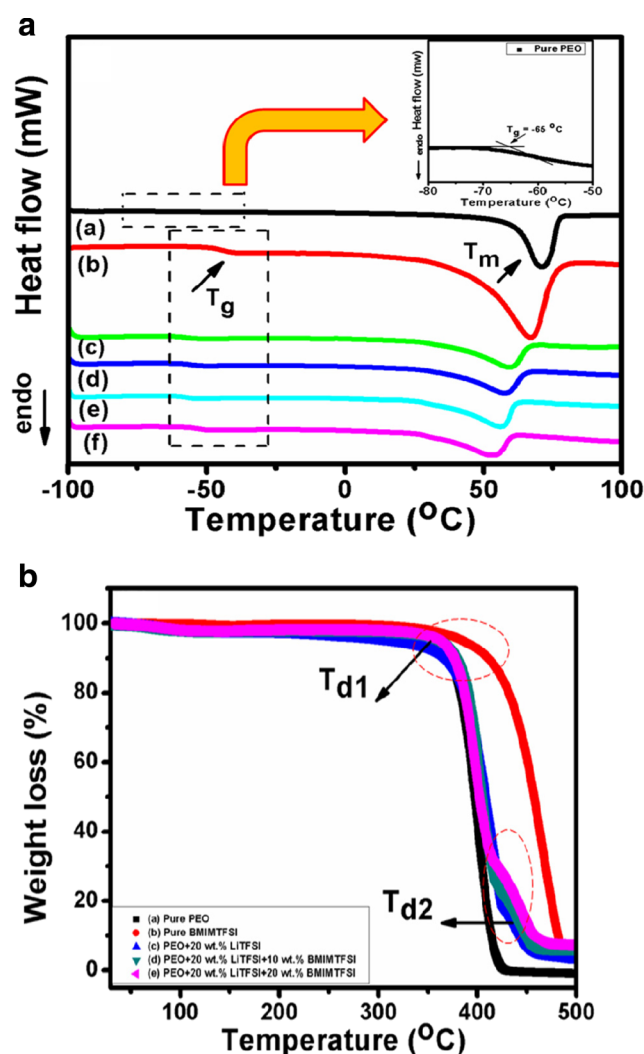
Fig. 1 **a** DSC thermograms of pristine PEO (*a*) and PEO + 20 wt.% LiTFSI and PEO + 20 wt.% LiTFSI + x wt.% BMIMTFSI (*b*), where $x = 5$ (*c*), $x = 10$ (*d*), $x = 15$ (*e*), and $x = 20$ (*f*). **b** TGA thermograms of pristine PEO (*a*), pristine BMIMTFSI (*b*), and PEO + 20 wt.% LiTFSI and PEO + 20 wt.% LiTFSI + x wt.% BMIMTFSI (*c*), where $x = 10$ (*d*) and $x = 20$ (*e*)

change with the amount of added IL. Therefore, the percentage degree of crystallinity has been evaluated by knowing the values of melting heat (ΔH_m) of polymer electrolyte to the melting ($\Delta H_m^o = 213$ J/g) of 100% crystalline PEO phase using the following relation:

$$\Delta H = \left(\frac{\Delta H_m}{\Delta H_m^o} \right) \times 100\% \qquad (2)$$

Different thermal parameters such as glass transition temperature, melting temperature and percentage degree of crystallinity of pristine PEO along with various polymer electrolytes containing different amounts of BMIMTFSI are given in Table 1. From this, we can see that on increasing the concentration of BMIMTFSI into PEO + 20 wt.% LiTFSI polymer electrolyte, the percentage degree of crystallinity decreases significantly and reaches to 26% for SPE that contains 20 wt.% BMIMTFSI [30].

The thermal stabilities of pure PEO, BMIMTFSI and polymer electrolytes ((PEO + 20 wt.% LiTFSI) + x wt.% BMIMTFSI for x = 0, 10, and 20) have been observed by TGA as shown in Fig. 1b. Figure 1b (a and b), respectively, shows the TGA curves of pristine polymer PEO and IL BMIMTFSI. Figure 1b (c–e) shows the TGA curves of the SPEs (PEO + 20 wt.% LiTFSI) + x wt.% BMIMTFSI for x = 0, 10, and 20. The pure PEO and pure BMIMTFSI were decomposed in single step with decomposition temperatures of 400 and 460 °C, respectively, as observed from Fig. 1b (a and b). On adding 20 wt.% LiTFSI, salt in the polymer PEO, two decompositions were obtained as indicated by T_{d1} and T_{d2} and shown in Fig. 1b (c) [18]. Furthermore, two decomposition peaks were also found upon incorporation of different amounts of BMIMTFSI to the SPE, PEO + 20 wt.% LiTFSI (see Fig. 1b (c–e)) at slightly lower temperatures [11, 34]. From these observations, we conclude that all the prepared Li-ion conducting SPEs are thermally stable up to ~350 °C, which is suitable for high-temperature range of operation for Li-ion rechargeable batteries.

Table 1 Melting temperature (T_m), glass transition temperature (T_g), and degree of crystallinity (X_c) of the membranes for different values of (PEO + 20 wt.% LiTFSI) + x wt.% of BMIMTFSI, where x = 0, 5, 10, 15, and 20 obtained by DSC

Serial no.	Sample name	T_m	T_g	X_c (%)
1	Pure PEO	70	−65	80
2	PEO + 20 wt.% LiTFSI	67	−40	70
3	PEO + 20 wt.% LiTFSI + 5 wt.% IL	59	−53	31
4	PEO + 20 wt.% LiTFSI + 10 wt.% IL	57	−51	29
5	PEO + 20 wt.% LiTFSI + 15 wt.% IL	55	−59	27
6	PEO + 20 wt.% LiTFSI + 20 wt.% IL	52	−41	26

Structural investigations

Figure 2a (a–c) shows the SEM micrographs of pure PEO and prepared SPE membranes (PEO + 20 wt.% LITFSI) + x wt.% BMIMTFSI (where x = 0 and 20). The pristine polymer PEO shows rough surface morphology with larger number of crystalline domains as shown in Fig. 2a (a). When 20 wt.% LiTFSI was added to polymer PEO to form a polymer electrolyte, then decrements in the rough surface morphology along with decreased crystalline domains were observed [30, 32]. The incorporation of 20 wt.% of BMIMTFSI to the PEO + 20 wt.% LiTFSI results in a significant increase in smoother surface morphology. These results clearly indicate that the incorporation of IL BMIMTFSI in PEO + 20 wt.% LiTFSI polymer electrolyte increases the amorphous phase, which increases the flexibility of the polymeric chain.

The X-ray diffraction profiles of pure PEO and polymer electrolyte (PEO + 20 wt.% LiTFSI) containing different amounts of BMIMTFSI over the range of 2θ = 10°–50° are shown in Fig. 2b (a–f). Figure 2b (a) presents the XRD profile of pristine PEO, which shows sharp crystalline peaks in the vicinity of 2θ = 15° to 30° along with some weak peaks at 2θ~15°, 26°, 27°, 36° and 40°. It can also be seen that these crystalline peaks are riding over a broad halo, which confirms the semicrystalline nature of the polymer PEO [35]. When 20 wt.% of LiTFSI salt was added to the polymer PEO, the intensity of the halo increased, which corresponds to an increase in the amorphous phase of the polymer electrolyte [36]. Also, we found the appearance of some new peaks at 14°, 17°, 18°, 19°, 27°, 23°, 25°, 27° and 28° corresponding to the polymer-salt complex formation. From Fig. 2a (b), we have found that when 20 wt.% LiTFSI was mixed with polymer, a peak related to LiTFSI appeared at ~14°. But upon incorporation of BMIMTFSI into the PEO + 20 wt.% LiTFSI polymer electrolyte system, two things are observed: (a) the intensity of halo increased substantially and (b) relative intensities of the crystalline peaks are reduced.

The absence of characteristic peaks related to LiTFSI in the XRD profiles of the polymer electrolyte confirms the complete dissolution of lithium salt into the PEO matrix in the presence of IL. Furthermore, for higher content of BMIMTFSI in PEO + 20 wt.% LiTFSI SPE (say 20 wt.%), the intensities of crystalline peaks are significantly reduced as shown in Fig. 2b (f), which corresponds to the presence of greater amorphous phase.

The FTIR spectroscopy technique has been used to know the possible interaction of LiTFSI and/or BMIMTFSI with the polymer PEO backbone. Figure 3a (a–f) shows the FTIR spectra of pure polymer PEO, BMIMTFSI and PEO + 20 wt.% LiTFSI + x wt.% BMIMTFSI for x = 0, 5, 10, 15 and 20 in the region 3500–400 cm^{-1}.

The interaction/complexation between the polymer PEO and cations of lithium salt LiTFSI or IL BMIMTFSI results some

Fig. 2 **a** SEM micrograph of pristine PEO (*a*), PEO + 20 wt.% LiTFSI (*b*) and PEO + 20 wt.% LiTFSI + 20 wt.% BMIMTFSI (*c*). **b** XRD pattern of pristine PEO (*a*) and PEO + 20 wt.% LiTFSI and (PEO + 20 wt.% LiTFSI) + *x* wt.% BMIMTFSI (*b*), where *x* = 5 (*c*), *x* = 10 (*d*), *x* = 15 (*e*) and *x* = 20 (*f*)
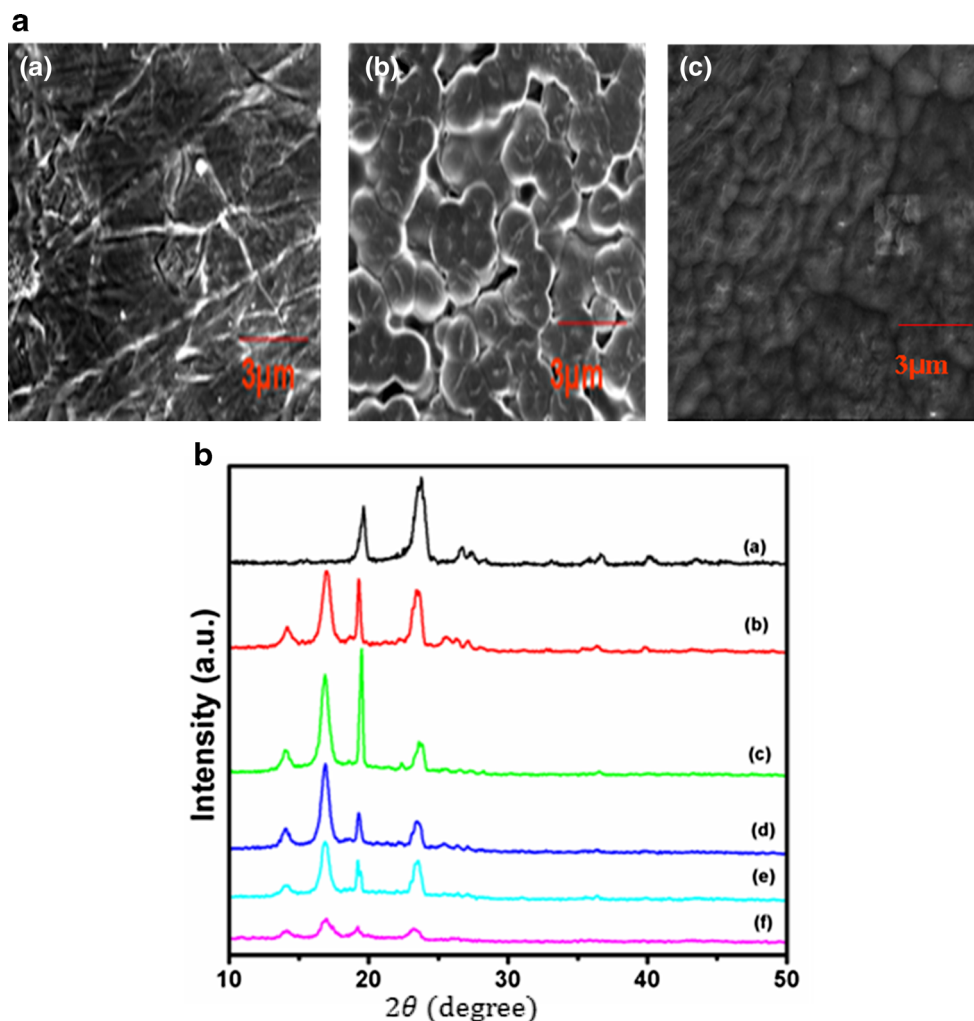

prominent change in two regions mainly: (i) 1000–1200 cm^{-1} related to the vibrations of C–O–C group present in PEO and (ii) 3000–3200 cm^{-1} related to the C–H stretching vibration of BMIMTFSI. The C–O–C-related vibrations of pure PEO appear as a group of three bands at 1060, 1116, and 1151 cm^{-1}. On incorporation of BMIMTFSI, IL in the PEO-LiTFSI complex system, slight shifting in the C–O–C-related bands of PEO was observed as shown in Fig. 3 (b), which indicates that there is a interaction between the C–O–C group of polymer PEO and the cations of salt (Li$^+$) and/or IL (BMIM$^+$) [37, 38]. The intensity of the peak at 1060 cm^{-1} related to C–O–C vibration of PEO increases with the concentration of BMIMTFSI in the PEO-LiTFSI polymer electrolyte system, suggesting that C–O–C group of polymer PEO is largely affected due to large size of TFSI anion at higher concentration of IL [39]. From Fig. 3a, it can also seen that CH$_2$-related bands of PEO at 843 and 948 cm^{-1} are not found to change much upon incorporation of IL(BMIMTFSI) into PEO + 20 wt.% LiTFSI system [40]. The intensity of bands related to CH$_2$ wagging and twisting vibrations of PEO observed at 1281 cm^{-1} starts decreasing and bands shift towards lower wave number side upon

incorporation of BMIMTFSI to the PEO + 20 wt.% LiTFSI system and this effect is more pronounced at higher loading of IL BMIMTFSI. The C–H stretching vibrations of imidazolium cation ring of BMIMTFSI observed at ~3121 and 3157 cm^{-1} are also affected due to the interaction of the cation of IL (BMIM$^+$) with the polymer PEO backbone as shown in Fig. 3c. From above discussion, it can be concluded that salt or IL cation, i.e., Li$^+$ or BMIM$^+$ (IL), gets complexed with the C–O–C group of polymer PEO.
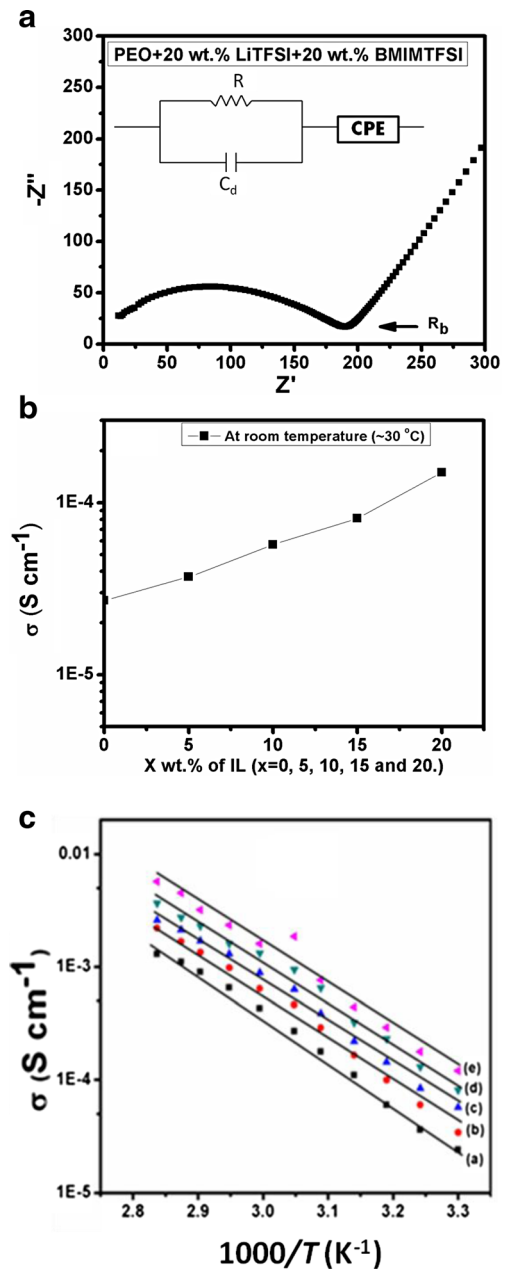
Temperature-dependent ionic conductivity studies

In our previous reported result, the ionic conductivity (σ) of pristine BMIMTFSI was found ~5.8 × 10^{-3} S cm^{-1} at room temperature (~30 °C), which increases with increasing temperature because of a decrease in viscosity at higher temperature [40], resulting in an easier ionic transport at higher temperatures due to increase in the ionic mobility (μ) of IL charge carriers [19].

Figure 4a shows the typical Nyquist plot and its equivalent circuit (inset of Fig. 4a of SPE (PEO + 20 wt.% LiTFSI +

a

b

c
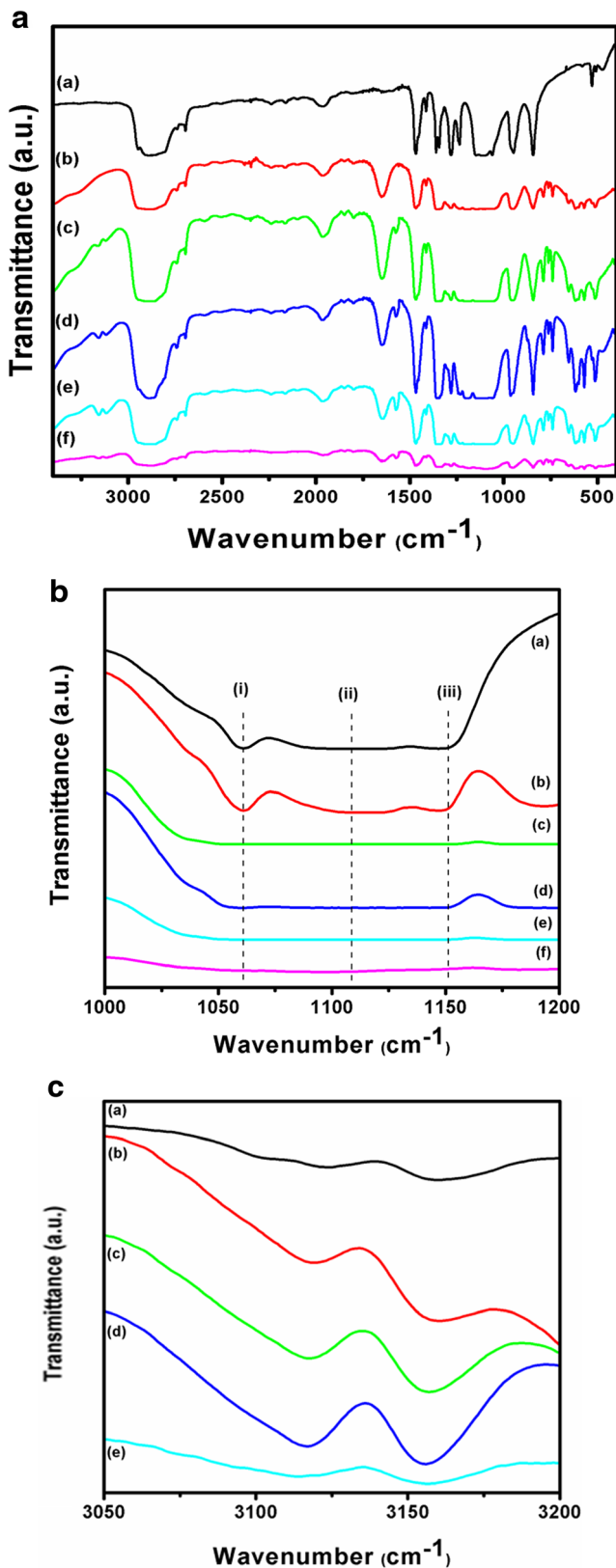
◀ **Fig. 3** **a** FTIR spectra of pristine PEO (*a*) and PEO + 20 wt.% LiTFSI and PEO + 20 wt.% LiTFSI + *x* wt.% BMIMTFSI (*b*), where *x* = 5 (*c*), *x* = 10 (*d*), *x* = 15 (*e*) and *x* = 20 (*f*) in the range of 3500 to 400 cm^{-1}. **b** FTIR spectra of pristine PEO (*a*) and PEO + 20 wt.% LiTFSI and PEO + 20 wt.% LiTFSI + *x* wt.% BMIMTFSI (*b*), where *x* = 5 (*c*), *x* = 10 (*d*), *x* = 15 (e) and *x* = 20 (*f*) in the range of 1000 to 1200 cm^{-1}. **c** FTIR spectra of pristine BMIMTFSI (*a*) and PEO + 20 wt.% LiTFSI (*c*) (PEO + 20 wt.% LiTFSI) + *x* wt.% BMIMTFSI, where *x* = 5 (*b*), *x* = 10 (*c*), *x* = 15 (*d*) and *x* = 20 (*e*) in the range of 3000 to 3200 cm^{-1}

a

b

c

Fig. 4 **a** Typical Nyquist plots of (PEO +20% LiTFSI) + 20% BMIMTFSI at room temperature and its equivalent circuit (inset of the figure). **b** Composition-dependent ionic conductivity for polymer electrolyte membranes (PEO + 20 wt.% LiTFSI) + *x* wt.% of BMIMTFSI, where *x* = 0, 5, 10, 15 and 20 at 30 °C. **c** Temperature-dependent ionic conductivity of the polymer electrolyte membranes PEO + 20 wt.% LiTFSI and (PEO + 20 wt.% LiTFSI) + *x* wt.% BMIMTFSI (*a*), where *x* = 5 (*b*), *x* = 10 (*c*), *x* = 15 (*d*) and *x* = 20 (*e*)

20 wt.% BMIMTFSI)) membrane at room temperature. From which, the value of bulk resistance was estimated.

The composition-dependent ionic conductivity of (PEO + 20 wt% LiTFSI) + x wt.% BMIMTFSI for x = 0, 5, 10, 15, and 20 at room temperature is shown in Fig. 4b. It can be seen that with increasing content of IL into the PEO + 20 wt.% LiTFSI system, ionic conductivity increases and attains a maximum value of ~1.5 × 10^{-4} S cm^{-1} for 20 wt.% of IL loading at ~30 °C. This increase in conductivity of polymer electrolyte with the concentration of IL (BMIMTFSI) is because of the increase in the amorphous phase of polymer electrolytes due to the plasticization effect of IL BMIMTFSI [41, 42].

The temperature-dependent ionic conductivity of SPEs (PEO+ 20 wt.% LiTFSI) + x wt.% BMIMTFSI for x = 0, 5, 10, 15 and 20 in the range of 30–70 °C is shown in Fig. 4c. It has been found that the ionic conductivity increases linearly with temperature and follows Arrhenius-type thermally activated behavior as [27]

$$\sigma = \sigma_o \exp\left(\frac{-E_a}{kT}\right) \tag{3}$$

where E_a is the activation energy, σ_o is the pre-exponential factor and k is the Boltzmann constant. Using Eq. (3), the activation energy for all the polymer electrolytes containing different amounts of BMIMTFSI has been evaluated from the slope of the plot. The value of E_a for PEO + 20 wt.% LiTFSI polymer electrolyte is found to be ~0.49 eV and starts to decrease with the addition of BMIMTFSI and reached the lowest value (~0.17 eV) for the highest loading of IL (20 wt.% IL) in the PEO + 20 wt.% LiTFSI SPE [43, 44]. This decrease in the activation energy (E_a) of SPE may be due to increased ionic transport as well as increase in the number of mobile charge carriers [30, 31]. In order to explain the ionic transport behavior in SPE, a phenomenological model has been proposed as shown in Fig. 5. Figure 5 (a) shows the semicrystalline nature of polymer PEO matrix; with the addition of 20 wt.% LiTFSI salt, the polymeric chain becomes more flexible (see Fig. 5 (b)). Furthermore, on incorporation of high IL content (20 wt.% BMIMTFSI) into the polymer-salt system, the SPE membrane becomes more flexible and gives higher conductivity [40].

Transference number

Figure 6a shows the total ionic transference number of prepared SPE evaluated by using the DC polarization technique. In this process, the SPE is sandwiched between two stainless steel (SS) electrodes and variation of current is recorded as a function of time. The total ionic transference number (t_{ion}) has been calculated using the following expression [30, 34]:

$$t_{ion} = 1 - \frac{I_e}{I_t} \tag{4}$$

where I_t and I_e are the total and steady state currents, respectively. t_{ion} of SPE was found to be ~0.98. This evaluated value of t_{ion} indicates that the overall conductivity is mainly contributed by the ions. But from application point of view, the cationic transference number (t_{Li^+}) is an important parameter to check the performance of polymer electrolytes. The Li-cationic transference number (t_{Li^+}) of the SPE PEO + 20 wt.% LiTFSI + 20 wt.% BMIMTFSI was calculated by a combined AC/DC technique. Figure 6b shows a typical plot of current vs. time for the symmetrical cell Li | SPE | Li. Inset of Fig. 6b shows the resistance of the cell before and after polarization. The t_{Li^+} is calculated by using the following equation [44, 45]:

$$t_{Li^+} = \frac{I_s(\Delta V - R_o I_o)}{I_o(\Delta V - R_s I_s)} \tag{5}$$

where I_o and I_s are the initial and steady state currents, respectively and R_o and R_s are the cell resistances before and after polarization. From Eq. (5), t_{Li^+} has been found to be ~0.27 [46–49].

Fig. 5 Schematic representation to understand the ionic transport behavior of pristine PEO and SPEs PEO + 20 wt.% LiTFSI and PEO + 20 wt.% LiTFSI + 20 wt.% BMIMTFSI at room temperature (~30 °C)
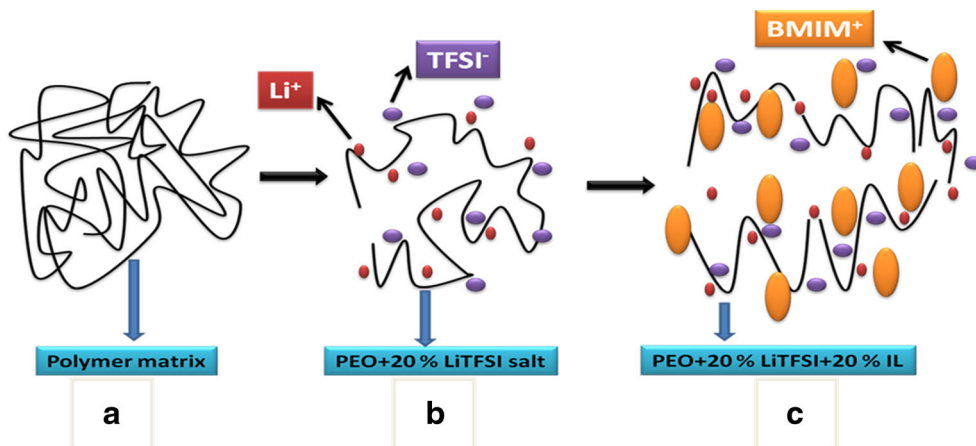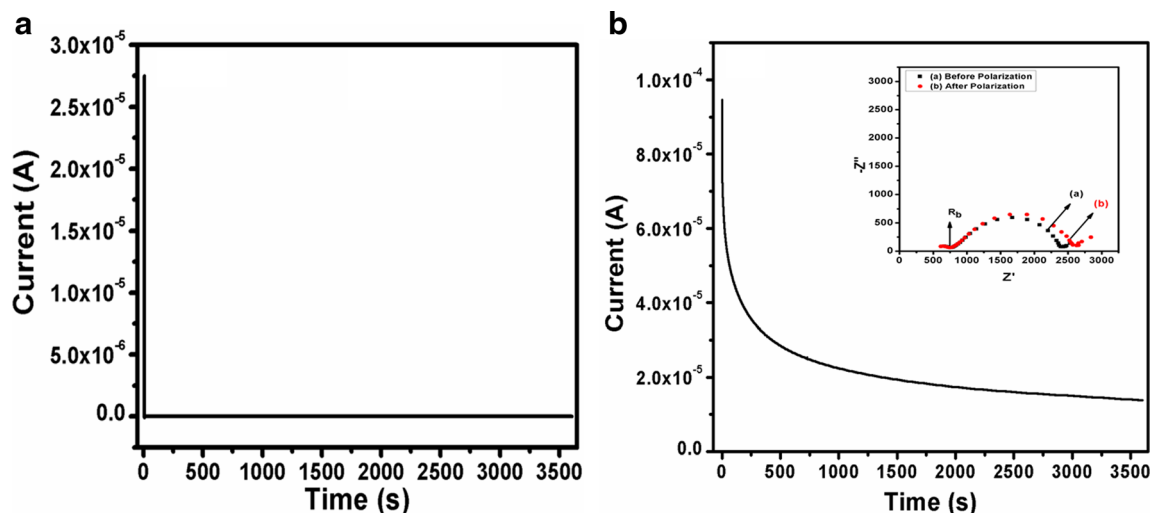
Fig. 6 Chronoamperometric curve at an applied voltage of 10 mV of the cell **a** SS | SPE | SS and **b** Li | SPE | Li at room temperature (~30 °C). *Inset* of **b** is the impedance plot of the cell Li | SPE | Li at room temperature before and after polarization

Electrochemical stability

To know the electrochemical potential window of optimized concentration of BMIMTFSI IL-based, Li-ion conducting SPE, LSV and CV have been performed. In this process, Li metal has been taken as reference and counterelectrode and $LiMn_2O_4$ as working electrode. Figure 7a shows the anodic electrochemical stability of fabricated cell Li | PEO + 20 wt.% LiTFSI + 20 wt.% BMIMTFSI | $LiMn_2O_4$ examined by linear sweep voltammetry. It can be seen from Fig. 7a that a wide electrochemical stability window up to ~4 V is obtained [50]. This observed wide electrochemical window is suitable for application in electrochemically stable Li-rechargeable batteries.

Figure 7b shows the cyclic voltammetry curve of Li | SPE | $LiMn_2O_4$ cell within the voltage range of 2.8 to 4.4 V at room temperature with scan rate of 0.01 V s^{-1}. As seen from Fig. 7b, each CV curve of the prepared cell shows that the intercalation/deintercalation of Li$^+$ from $LiMn_2O_4$ cathode has been taken at voltage of 3.8 and 4.1 V, respectively.

Charge-discharge studies

To investigate the application of optimized SPE, it is sandwiched between Li anode and $LiMn_2O_4$ cathode and the performance of the cell (Li | SPE | $LiMn_2O_4$ schematically shown in Fig. 8) has been recorded at room temperature with 0.2 C rate as shown in Fig. 9a. The lower and upper cutoff potentials of the cell were fixed at 2.8 and 4.5 V, respectively, to avoid the decomposition of electrolyte. A flat plateau has been observed around 3.8 V. This shows that the Li intercalation/deintercalation has been taken in this voltage range (~3.8 V) [51, 52]. Figure 9b shows the cyclic performance of cell Li | SPE | $LiMn_2O_4$.
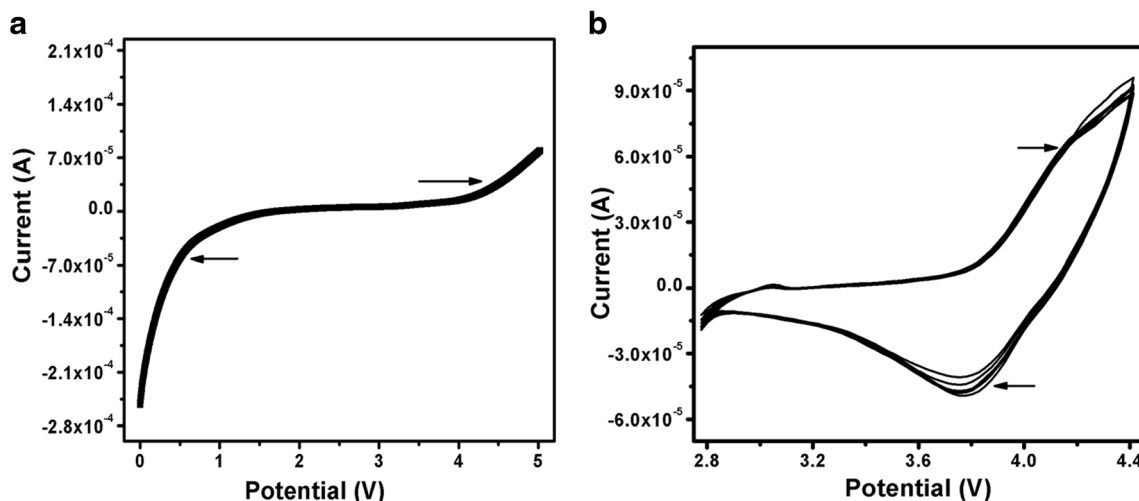
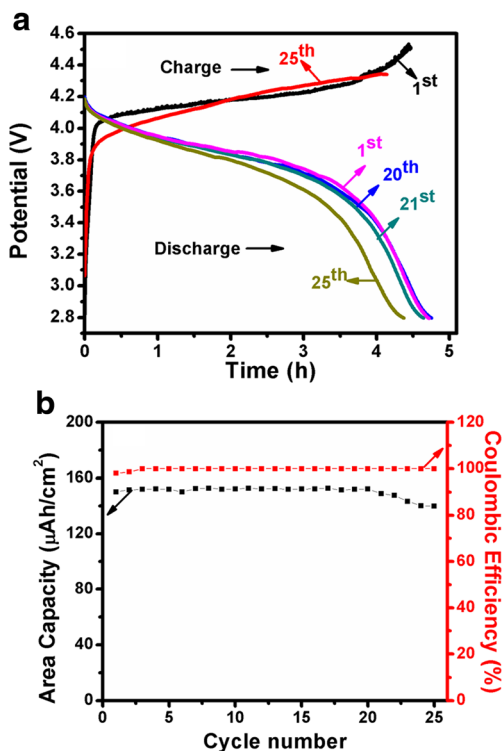**Fig. 7** **a** LSV of assembled battery Li | SPE | $LiMn_2O_4$ at scan rate of 0.01 V/s. **b** CV profiles of Li | SPE | $LiMn_2O_4$ battery at different scan rate of 0.01 V/s in the range of 4.4 to 2.8 V
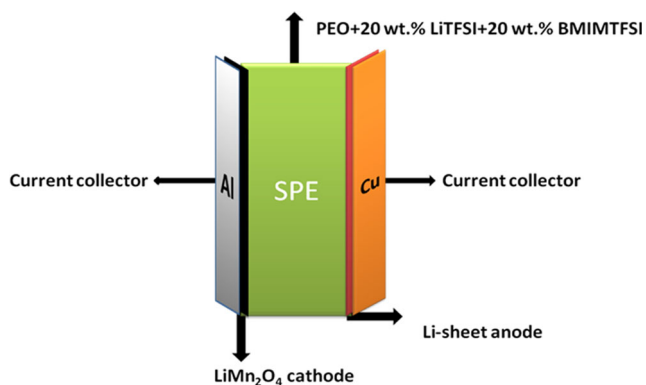
Fig. 8 Schematic illustration of prepared cell Li | SPE | LiMn$_2$O$_4$

Figure 9b demonstrates the cyclic performance of the cell Li | SPE | LiMn$_2$O$_4$. From this figure, it is observed that the areal discharge capacity remains constant at ~152 μAh/cm^2 up to 20th cycle at room temperature; this may be because solid electrolyte interface (SEI) acts as a protective layer at electrode-electrolyte interface, which prevents the capacity fading up to 20 cycles. After 20 cycles, the areal discharge capacity fading occurred slowly and became 140 μAh/cm^2 at 25th cycle. It may be due to the side reactions occurring at the electrode-electrolyte interface during intercalation/deintercalation process

[53–56]. Also, we have calculated the Coulombic efficiency by using the following equation:

$$\eta = \left(\frac{\Delta Q_d}{\Delta Q_c} \right) \times 100\% \qquad (6)$$

where $\Delta Q_d = (Q_f - Q_i)$ and $\Delta Q_c = (Q_f - Q_i)$ are the amounts of charge during discharge and charge cycles, respectively, and by using above Eq. (6), we have determined the cell Coulombic efficiency of the battery for 25 cycles. The Coulombic efficiency of the Li | SPE | LiMn$_2$O$_4$ is nearly 100% except for first cycle. It is less for the first cycle due to the formation of a protective SEI film on the electrode-electrolyte interface [30, 53]. Resulting cycling performance reflects their higher reversible charge-discharge ability. We obtained a better interfacial property towards the lithium-metal anode, and cycling ability of the cell shows good results at room temperature. Therefore, this optimized high-content, IL-based SPE can be employed both as a separator and electrolyte for application in Li-rechargeable batteries and suggests that the cycling behavior of this battery system is good.

Conclusions

The BMIMTFSI IL-based polymer electrolytes (PEO + 20 wt.% LiTFSI) + x wt.% BMIMTFSI for x = 0, 5, 10, 15 and 20 were prepared by solution-casting technique, and thermal behavior, ionic conductivity, complexation, electrochemical stability, transference number (ionic and cationic), and interfacial properties with Li/LiMn$_2$O$_4$ cell were studied by using different techniques such as DSC, TGA, EIS, SEM, XRD, CV, chronoamperometry and chronocharge-discharge. SEM, XRD, and FTIR results show that the ions of LiTFSI/BMIMTFSI interact with the C–O–C group of polymer PEO, and result enhanced polymeric chain flexibility and hence the ionic conductivity. DSC result shows that the degree of crystallinity decreases with the incorporation of BMIMTFSI IL in the polymer-salt complex system, and TGA confirms the excellent thermal stability which is up to ~350 °C. The incorporation of BMIMTFSI IL into the polymer-salt complex system results in a significant increase in ionic conductivity and increases with increase in temperature and reaches ~2.2 × 10^{-3} S cm^{-1} at 70 °C for (PEO + 20 wt.% LiTFSI) + 20 wt.% BMIMTFSI. CV study shows the suitability of SPEs containing BMIMTFSI IL for lithium polymer battery application with well-defined redox potentials and high-voltage window for prepared cell. The presence of IL in SPEs significantly reduces the resistance of the cell and also helps to achieve faster lithium electrode stabilization. The optimized SPEs with good ionic conductivity and mechanical integrity show good Columbic efficiency (100% up to 25 cycles) and

Fig. 9 a Charge-discharge characteristics for 1st, 20th, 21st and 25th cycles between ~4.5 and 2.8 V. **b** Charge-discharge capacities and Coulombic efficiencies of cell Li | SPE | LiMn$_2$O$_4$ during cycling of charge-discharge for 25 cycles

stable cyclic performance for the prepared cell Li | SPE | LiMn$_2$O$_4$ at room temperature (30 °C).

References

1. Meyer WH (1998) Polymer electrolytes for lithium-ion batteries. Adv Mater 10:439
2. Tsao C-H, Hsiao Y-H, Hsu C-H, Kuo P-L (2016) Toward dendrite-free lithium deposition via structural and interfacial synergistic effects of 3D graphene@ Ni scaffold. ACS Appl Mater Interfaces 8:15216–15224
3. Lin F, Markus IM, Nordlund D, Weng TC, Asta MD, Xin HL, Doeff MM (2014) Surface reconstruction and chemical evolution of stoichiometric layered cathode materials for lithium-ion batteries. Nat Commun 5:3529
4. Luo W, Zhou L, Fu K, Yang Z, Wan J, Manno M, Yao Y, Zhu H, Yang B, Hu L (2015) A thermally conductive separator for stable Li metal anodes. Nano Lett 15:6149–6154
5. Berthier C, Gorecki W, Minier M, Armand MB, Chabgno JM, Rraiagud P (1983) Microscopic investigation of ionic conductivity in alkali metal salts-poly(ethylene oxide) adducts. Solid State Ionics 11:91–95
6. Li F, Gong Y, Jia G, Wang Q, Peng Z, Fan W, Bai B (2015) A novel dual-salts of LiTFSI and LiODFB in LiFePO4-based batteries for suppressing aluminum corrosion and improving cycling stability. J Power Sources 295:47–54
7. Wang X, Hou Y, Zhu Y, Wu Y, Holze R (2013) An aqueous rechargeable lithium battery using coated Li metal as anode. Scientific reports 3:1401
8. Zhao R, Zhang S, Liu J, Gu J (2015) A review of thermal performance improving methods of lithium ion battery: electrode modification and thermal management system. J Power Sources 299:557–577
9. Yamada I, Abe T, Iriyama Y, Ogumi Z (2003) Lithium-ion transfer at LiMn$_2$O$_4$ thin film electrode prepared by pulsed laser deposition. Electrochem Commun 5:502–505
10. Lu J, Yan F, Texter J (2009) Advanced applications of ionic liquids in polymer science. Prog Polym Sci 34:431–448
11. Shui Zhang S (2006) An unique lithium salt for the improved electrolyte of Li-ion battery. Electrochem Commun 8(9):1423–1428
12. Scrosati B (2011) History of lithium batteries. J Solid State Electrochem 15:1623–1630
13. Croce F, Curini R, Martinelli A, Persi L, Ronci F, Scrosati B, Caminiti R (1999) Physical and chemical properties of nanocomposite polymer electrolytes. J Phys Chem B 103:10632–10638
14. Rajendran S, Sivakumar M, Subadevi R (2004) Investigations on the effect of various plasticizers in PVA–PMMA solid polymer blend electrolytes. Mater Lett 58:641–649
15. Appetecchi GB, Crore F, Scrosati B (1995) Kinetics and stability of the lithium electrode in poly(methylmethacrylate)-based gel electrolytes. Electrochim Acta 40:991–997
16. Dell R (2000) Batteries fifty years of materials development. Solid State Ionics 134:139–158
17. Singh MP, Singh RK, Chandra S (2014) Ionic liquids confined in porous matrices: physicochemical properties and applications. Prog Mater Sci 64:73–120
18. Nicotera I, Oliviero C, Henderson WA, Appetecchi GB, Passerini S (2005) NMR investigation of ionic liquid-LiX mixtures: pyrrolidinium cations and TFSI anions. J Phys Chem B 109:22814–22819
19. Chaurasia SK, Singh RK, Chandra S (2011) Structural and transport studies on polymeric membranes of PEO containing ionic liquid, EMIM-TY: evidence of complexation. Solid State Ionics 183:32–39
20. Eshetu GG, Armand M, Ohno H, Scrosati B, Passerini S (2016) Ionic liquids as tailored media for the synthesis and processing of energy conversion materials. Energy Environ Sci 9:49–61
21. Fung YS, Zhou RQ (1999) Room temperature molten salt as medium for lithium battery. J. Power Sources 81:891–895
22. Garcia B, Lavallee S, Perron G, Michot C, Armand M (2004) Room temperature molten salts as lithium battery electrolyte. Electrochim Acta 49:4583–4588
23. Sakaebe H, Matsumoto H (2003) N-methyl-N-propylpiperidinium bis (trifluoromethanesulfonyl) imide (PP$_{13}$–TFSI)—novel electrolyte base for Li battery. Electrochem Commun 5:594–598
24. Yuan LX, Feng JK, Ai XP, Cao YL, Chen SL, Yang HX (2006) Improved dischargeability and reversibility of sulfur cathode in a novel ionic liquid electrolyte. Electrochem Commun 8:610–614
25. Sato T, Maruo T, Marukane S, Takagi K (2004) Ionic liquids containing carbonate solvent as electrolytes for lithium ion cells. J. Power Sources 138:253–261
26. Kim KS, Park SY, Choi S, Lee H (2006) Ionic liquid–polymer gel electrolytes based on morpholinium salt and PVDF (HFP) copolymer. J. Power Sources 155:385–390
27. Shin JH, Henderson WA, Appetecchi GB, Alessandrini F, Passerini S (2005) Recent developments in the ENEA lithium metal battery project. Electrochim Acta 50:3859–3865
28. Shin JH, Henderson WA, Passerini S (2003) Ionic liquids to the rescue? Overcoming the ionic conductivity limitations of polymer electrolytes. Electrochem Commun 5:1016–1020
29. Singh VK, Shalu, Kumar Chaurasia S, Singh RK (2016) Development of ionic liquid mediated novel polymer electrolyte membranes for application in Na-ion batteries. RSC Adv 6:40199–40210
30. Yang H, Zhuang GV, Ross PN (2006) Thermal stability of LiPF$_6$ salt and Li-ion battery electrolytes containing LiPF6. J Power Sources 161(1):573–579
31. Choi J-W, Cheruvally G, Kim Y-H, Kim J-K, Manue J, Raghavan P, Ahn J-H, Kim K-W, Ahn H-J, Choi DS, Song CE (2007) Poly(ethylene oxide)-based polymer electrolyte incorporating room-temperature ionic liquid for lithium batteries. Solid State Ionics 178:1235–1241
32. Chaurasia SK, Saroj AL, Shalu SVK, Tripathi AK, Gupta AK, Verma YL, Singh RK (2015) Studies on structural, thermal and AC conductivity scaling of PEO-LiPF$_6$ polymer electrolyte with added ionic liquid [BMIMPF$_6$]. AIP Adv 5:077178
33. Li LF, Zhou SS, Han HB, Li H, Nie J, Armand M, Zhou ZB, Huang XJ (2011) Transport and electrochemical properties and spectral features of non-aqueous electrolytes containing LiFSI in linear carbonate solvents. J Electrochem Soc 158(2):A74–A82
34. Chen Z, Lu WQ, Liu J, Amine K (2006) LiPF$_6$/LiBOB blend salt electrolyte for high-power lithium-ion batteries. Electrochim Acta 51(16):3322–3326
35. de Freitas JN, Nogueira AF, De Paoli MA (2009) New insights into dye-sensitized solar cells with polymer electrolytes. J Mater Chem 19:5279–5294
36. Cheng H, Zhu C, Huang B, Lu M, Yang Y (2007) Synthesis and electrochemical characterization of PEO-based polymer electrolytes with room temperature ionic liquids. Electrochim Acta 52:5789–5794
37. Chaurasia SK, Singh RK, Chandra S (2011) Ion–polymer and ion–ion interaction in PEO-based polymer electrolytes having complexing salt LiClO$_4$ and/or ionic liquid, [BMIM][PF$_6$]. J Raman Spectrosc 42:2168–2172

38. Tian X, Jiang X, Zhu B, Xu Y (2006) Effect of the casting solvent on the crystal characteristics and pervaporative separation performances of P(VDF-co-HFP) membranes. J Membr Sci 279:479–486

39. Rao SS, Reddy MJ, Narsaiah EL, Rao S (1995) Development of electrochemical cells based on (PEO + $NaYF_4$) and (PEO + KYF_4) polymer electrolytes. J Mater Sci Eng B 33:173–177

40. Shalu, Singh VK, Singh RK (2015) Development of ion conducting polymer gel electrolyte membranes based on polymer PVDF-HFP, BMIMTFSI ionic liquid and the Li-salt with improved electrical, thermal and structural properties. J Mater Chem C 3:7305–7318

41. Manning JP, Frech CB, Fun BM, Frech RE (1991) Multinuclear nuclear magnetic resonance relaxation investigations of poly(propylene oxide) complexed with sodium trifluoromethanesulphonate. Polymer 32:2939–2946

42. Fan L, Nan CW, Zhao S (2003) Effect of modified SiO_2 on the properties of PEO-based polymer electrolytes. Solid State Ionics 164:81–86

43. Stoeva Z, Martin-Litas I, Staunton E, Andreev YG, Bruce PG (2003) Ionic conductivity in the crystalline polymer electrolytes PEO_6:$LiXF_6$, X = P, As. Sb J Am Chem Soc 125:4619–4626

44. Chandra A, Chandra A, Thakur K (2016) Synthesis and ion conduction mechanism on hot-pressed sodium ion conducting nanocomposite polymer electrolytes. Arab J Chem 9:400–407

45. Moreno JS, Armand M, Berman MB, Greenbaum GS, Scrosati B, Panero S (2014) Composite $PEOn$:NaTFSI polymer electrolyte: preparation, thermal and electrochemical characterization. J Power Sources 248:695–702

46. Hasa I, Passerini S, Hassoun J (2016) Characteristics of an ionic liquid electrolyte for sodium-ion batteries. J Power Sources 303:203–207

47. Ghosh A, Wang C, Kofinas P (2010) PMMA–LiBOB gel electrolyte for application in lithium ion batteries. J Electrochem Soc 157:846

48. Fasciani C, Panero S, Hassoun J, Scrosati B (2015) Novel configuration of poly(vinylidenedifluoride)-based gel polymer electrolyte for application in lithium-ion batteries. J Power Sources 294:180–186

49. Croce F, Settimi L, Scrosati B (2006) Superacid ZrO_2-added, composite polymer electrolytes with improved transport properties. Electrochem Commun 8:364–368

50. Nozaki H, Nagaoka K, Hoshi K, Ohta N, Inagaki M (2009) Carbon-coated graphite for anode of lithium ion rechargeable batteries: carbon coating conditions and precursors. J Power Sources 194:486–493

51. Kim J-K, Mueller F, Kim H, Jeong S, Park J-S, Passerini S, Kim Y (2016) Eco-friendly energy storage system: seawater and ionic liquid electrolyte. ChemSusChem 9:42–49

52. Togasaki N, Momma T, Osaka T (2016) Enhanced cycling performance of a Li metal anode in a dimethylsulfoxide-based electrolyte using highly concentrated lithium salt for a lithium−oxygen battery. J Power Sources 307:98–104

53. Li Q, Ardebili H (2016) Flexible thin-film battery based on solid-like ionic liquid-polymer electrolyte. J Power Sources 303:17–21

54. Navarra MA, Manzi J, Lombardo L, Panero S, Scrosati B (2011) Ionic liquid-based membranes as electrolytes for advanced lithium polymer batteries. ChemSusChem 4:125–130

55. Khan RNN, Mahmood N, Lv C, Sima G, Zhang J, Hao J, Hou Y, Wei Y (2014) Pristine organo-imido polyoxometalates as an anode for lithium ion batteries. RSC Adv 4:7374

56. Varzi A, Ramirez-Castro C, Balducci A, Passerini S (2015) Performance and kinetics of $LiFePO_4$–carbon bi-material electrodes for hybrid devices: a comparative study between activated carbon and multi-walled carbon nanotubes. J Power Sources 273:1016–1022